A Localized Linearized ROF Model for Surface Denoising

Shingyu Leung*

August 7, 2008

Abstract

1 Introduction

CT/MRI scan becomes a very important tool in visualizing body parts. In clinical evaluation and treatment planning, the vessels or organs are reconstructed by image segmentation from a huge three dimensional data set. Typical data sets can be very large with up to thousand pixels in each direction nowadays to give a very good resolution in each two dimensional slice.

Various segmentation methods have been proposed. One approach is to construct a level set function to implicitly represent the desire structure, including Chan-Vese, geodesic active contour, non-local level set, and etc. However, these PDE-based methods are usually computationally expensive. Since one usually solves their corresponding Euler-Lagrange equation using gradient descent, the minimizer of these energies are obtained by finding the steady state solution to these partial differential equations. Another disadvantage of these methods is that it could be too expensive to store another three-dimensional data for the level set function.

Yet the most widely used method is still to simply look at a particular intensity level of the data set. This is due to the fact that different tissues will in general give a significant different intensity level in the image. However, the data set obtained from MRI might be seriously polluted and this reconstruction will produce many unwanted tiny features which cover up the important features.

[subcell resolution]

*Department of Mathematics, UCI, Irvine, CA 92697-3875. Email: **syleung@math.uci.edu**

In this paper, we propose regularizing the intensities at pixels/voxels only in a neighborhood of the level surface from simple thresholding. Unlike usual segmentation method, we do not require storage of an additional data set for the surface. We first collect these voxels near the level surface and then modify their corresponding intensities by applying a linearized ROF regularization. This results in a system of linear equations which can be solved efficiently. Furthermore, since on each two dimensional slice the level surface is usually a curve, the regularization we made is minimal in the sense that the original and the modified data set should be indistinguishable when we look at these two dimensional slices. This leaves the medical doctor freedom to judge if any fine feature in these slices is important.

2 Localized ROF

Let $\Omega \subset \mathbb{R}^3$ be the whole three dimensional data set, u^* is the threshold level for intensity segmentation, $\mathcal{B}_{\mathbf{x},r_0}$ is a ball of radius r_0 centered at $\mathbf{x}$ and

$$\begin{aligned}\tilde{\Omega}_{r_0} &= \{\mathbf{x} : \exists \mathbf{y} \in \mathcal{B}_{\mathbf{x},r} \text{ such that } u_0(\mathbf{y}) = u^*\} \\ &= \{\mathbf{x} : \exists \mathbf{y}_1, \mathbf{y}_2 \in \mathcal{B}_{\mathbf{x},r} \text{ such that } [u_0(\mathbf{y}_1) - u^*] \cdot [u_0(\mathbf{y}_2) - u^*] < 0\} \qquad (1)\end{aligned}$$

is a radius r_0 neighborhood of the level surface $u_0^{-1}(u^*)$. The first definition above is a continuum definition for continuous domain, while the second one is more suitable for the current application where the intensity values are defined on discrete pixel/voxel locations.

Instead of applying the origin ROF model [3] everywhere in Ω, we restrict the regularization only to $\tilde{\Omega}$. This means we localize the original ROF energy to a neighborhood of the desire level surface, giving

$$\begin{aligned}E_{LROF}(u) &= \int_{\Omega} |\nabla u| + \frac{\lambda(\mathbf{x})}{2}(u-u_0)^2 \\ &= \int_{\tilde{\Omega}} |\nabla u| + \frac{\lambda_0}{2}(u-u_0)^2 \,, \qquad (2)\end{aligned}$$

where

$$\lambda(\mathbf{x}) = \begin{cases} \lambda_0 \geq 0 & \text{if } \mathbf{x} \in \tilde{\Omega}_{r_0} \\ \infty & \text{otherwise} \end{cases} \,. \qquad (3)$$

[limit cases when $\lambda_0 = 0$ or ∞.]

Theorem 2.1. *Consider the following two dimensional case with the initial intensity image given by*

$$u_0 = \chi_{\mathcal{B}_{r_1}} \,, \qquad (4)$$

where $\mathcal{B}_{r_1}$ is a ball of radius r_1 and χ is the characteristic function. Let $0 < u^* < 1$ be the desire threshold intensity and $\tilde{\Omega}_{r_0}$ is the neighborhood we are regularizing. If $r_1 < r_0$ and u is the minimizer to the ROF energy (2), then there exist $\lambda^* > 0$ such that

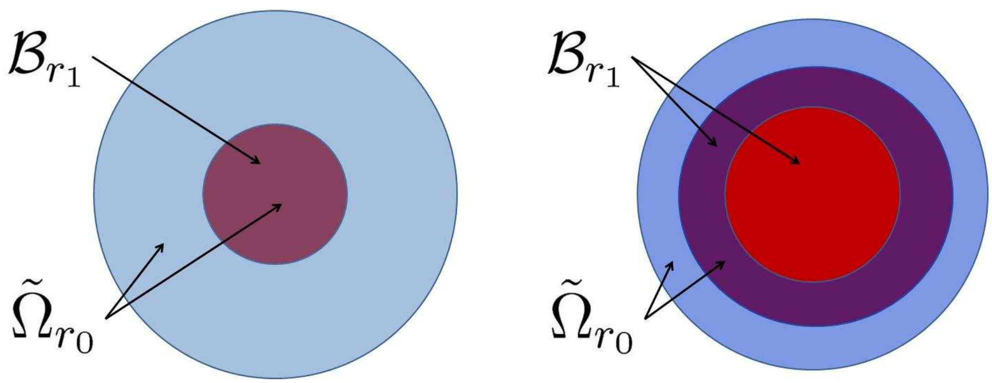

Figure 1: Setup for (left) Theorem 2.1 and (right) Theorem 2.2.

1. *if* $\lambda^* < \lambda_0$, $u^{-1}(u^*) = u_0^{-1}(u^*)$;
2. *if* $\lambda_0 < \lambda^*$, $u^{-1}(u^*)$ *is empty.*

Proof. The idea follows from the calculations in [2, 4]. The minimizer to the energy (2) can be explicitly defined in this case

$$u = \begin{cases} 0 & \text{if } 0 \le \lambda_0 \le \frac{1}{r_1} \\ \left(1 - \frac{1}{\lambda_0 r_1}\right) \chi_{\mathcal{B}_{r_1}} & \text{if } \lambda_0 > \frac{1}{r_1} \, . \end{cases} \tag{5}$$

Let

$$\lambda^* = \frac{1}{r_1(1 - u^*)} \, . \tag{6}$$

If $\lambda_0 < \lambda^*$, we have $u < u^*$ and therefore the simple segmentation using the threshold u^* will give the empty set. If $\lambda^* < \lambda_0$, $u(\mathcal{B}_{r_1}) = (1 - 1/\lambda_0 r_1) > u^*$ which gives the same segmentation as the original function u_0. □

Theorem 2.2. *Consider the following two dimensional case with the initial intensity image given by*

$$u_0 = \chi_{\mathcal{B}_{r_1}} \, , \tag{7}$$

where $\mathcal{B}_{r_1}$ *is a ball of radius* r_1 *and* χ *is the characteristic function. Let* $0 < u^* < 1$ *be the desire threshold intensity and* $\tilde{\Omega}_{r_0}$ *is the neighborhood we are regularizing. If* $r_0 < r_1$ *and* u *is the minimizer to the ROF energy (2), then* $u^{-1}(u^*) = u_0^{-1}(u^*)$.

These two theorems imply that any fine features in the observed data set will be removed only when its scale is smaller than the tube radius r_0 and with a regularization parameter λ_0 smaller than some critical λ^*. Moreover, if these features appear as a sudden change in the intensity, it will either be completely removed or remain unchanged. It will not be removed gradually by shrinking.

3 Localized Linearized ROF

[1] has recently proposed linearizing some nonlinear non-local filters not only to speed up the computations, but also to produce a better quality and fidelity images. The underlying observation is that the corresponding nonlinear version $u(t,\mathbf{x})$ goes away from the original data u_0, while the linearized version keeps the direct knowledge of u_0.

The original Euler-Lagrange equation for the above localized ROF is given by

$$u_t = \nabla \cdot \left(\frac{\nabla u}{|\nabla u|} \right) - \lambda_0 (u - u_0) \tag{8}$$

in $\tilde{\Omega}_{r_0}$ with $u = u_0$ for $\mathbf{x} \in \Omega \backslash \tilde{\Omega}_{r_0}$. Linearizing this equation gives

$$u_t = \nabla \cdot \left(\frac{\nabla u}{|\nabla u_0|} \right) - \lambda_0 (u - u_0) \tag{9}$$

with the corresponding energy

$$E_{LLROF} = \int_\Omega \frac{1}{2} \frac{|\nabla u|^2}{|\nabla u_0|} + \frac{\lambda(\mathbf{x})}{2} (u - u_0)^2 \,. \tag{10}$$

In fact, the minimizer to (10) can be found by simply solving the following linear inhomogeneous anisotropic Helmholtz equation in $\tilde{\Omega}$

$$\lambda_0 u - \nabla \cdot \left(\frac{\nabla u}{|\nabla u_0|} \right) = \lambda_0 u_0 \,. \tag{11}$$

Now we study some properties of these minimizers to the proposed localized linearized ROF energy (10).

Theorem 3.1. *Consider the following two dimensional case with the initial intensity image given by*

$$u_0 = \sqrt{x^2 + y^2} \,. \tag{12}$$

Let $u^* > 0$ be the desire threshold intensity and $\tilde{\Omega}_{r_0}$ is the neighborhood we are regularizing. If $r_0 < u^*$, the reconstruction surface $u^{-1}(u^*)$ lies inside $u_0^{-1}(u^*)$.

Proof. For a given threshold level $u^* > 0$, the level surface $u_0^{-1}(u^*)$ is a circle of radius u^*. The condition $r < u^*$ implies that the domain $\tilde{\Omega}_{r_0}$ is an annulus given by $\{u^* - r_0 < \sqrt{x^2 + y^2} < u^* + r_0\}$. Assuming the solution is independent of θ and is in the form of $u(r)$, equation (11) implies

$$u_{rr} + \frac{1}{r} u_r - \lambda_0 u = -\lambda_0 r \,, \tag{13}$$

with the boundary values $u(u^* - r_0) = u^* - r_0$ and $u(u^* + r_0) = u^* + r_0$. We first study two limit cases. If $\lambda_0 \to \infty$, the minimizer to (10) is $u = u_0$. For the other limit when $\lambda_0 = 0$, we have

$$u(r) = c_1 + c_2 \log(r) \,, \tag{14}$$

with $c_2 = 2r_0/[\log(u^*+r_0)-\log(u^*-r_0)] > 0$. Since $u'(r) = c_2/r > 0$ and $u''(r) = -c_2/r^2 < 0$, we conclude $u(r) > r$. This implies the original surface $u_0^{-1}(u^*)$ shrinks to $u^{-1}(u^*)$ for the case $\lambda_0 = 0$.

Now, introducing $v(r) = u(r) - r$, we have

$$v_{rr} + \frac{1}{r}v_r - \lambda_0 v = -\frac{1}{r}\,, \tag{15}$$

with the boundary values $v(u^* - r_0) = v(u^* + r_0) = 0$. The above analysis is therefore equivalent to say that $\lambda_0 = 0$ implies $v(r) > 0$ for $\forall r \in (u^* - r, u^* + r)$ and $\lambda_0 \to \infty$ implies $v(r) = 0$ for $\forall r \in (u^* - r, u^* + r)$.

Now we consider any finite $\lambda_0 > 0$. If the function $v(r)$ has a global minimum at r^* on $(u^* - r, u^* + r)$, we have $v(r^*) \leq 0$ and $v_r(r^*) = 0$.

1. $v(r^*) < 0$. Since $v_r(r^*) = 0$, we have $v_{rr}(r^*) \geq 0$. This gives

$$v_{rr}(r^*) + \frac{1}{r^*}v_r(r^*) - \lambda_0 v(r^*) > 0 \tag{16}$$

   which contradicts with (15).

2. $v(r^*) = 0$. Using (15), we have

$$v_{rr}(r^*) = \frac{-1}{r^*} < 0\,. \tag{17}$$

   This implies there exists $\tilde{r}$ in the neighborhood of r^* such that $f(\tilde{r}) < 0$, which contradicts with the assumption that $v(r^*)$ the a global minimum.

This implies that the global minimum of $v(r)$ are 0 only at $r = u^* \pm r_0$. We now conclude $v(r) > 0$ for $\forall r \in (u^* - r, u^* + r)$.

Figure 1 shows some numerical solutions to (15) for various λ_0. The top-most curve corresponds to the case when $\lambda_0 = 0$. As we increase λ_0, i.e. to reduce the regularization, the deviation of the solution $v(r)$ from zero reduces. Yet, it stays positive for all λ_0. As λ_0 tends to infinity, we have $v(r) \equiv 0$. Since $v(r) > 0$ for all $\lambda_0 > 0$, we have $u_0^{-1}(u^*)$ shrinks to $u^{-1}(u^*)$.

As a final remark to this case when $|\nabla u_0| = 1$, the proposed regularization is reduced to the following L_2 regularization

$$E_{L_2} = \int_\Omega \frac{1}{2}|\nabla u|^2 + \frac{\lambda(\mathbf{x})}{2}(u - u_0)^2\,. \tag{18}$$

$\square$

The amount how much the surface shrinks depends on the parameter λ_0.

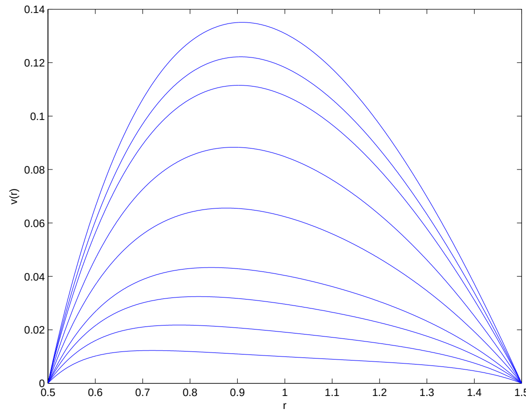

Figure 2: (Proof for 3.1) An illustration of $v(r)$ as λ_0 changes.

Theorem 3.2. *Consider the following two dimensional case with the initial intensity image given by*

$$u_0 = \sqrt{x^2 + y^2}\,. \tag{19}$$

Let $u^* > 0$ be the desire threshold intensity and $\tilde{\Omega}_{r_0}$ is the neighborhood we are regularizing. Let $\bar{u}$ be the minimizer to (10) for $\lambda_0 = 0$ and $\tilde{u}$ be the minimizer to the same energy for some other $\tilde{\lambda} > 0$. If $r_0 < u^*$, the reconstructed surface $\bar{u}^{-1}(u^*)$ lies inside $\tilde{u}^{-1}(u^*)$.

Proof. Let $w = \bar{u} - \tilde{u}$. We have

$$w_{rr} + \frac{1}{r} w_r - \tilde{\lambda}\tilde{u} = 0\,, \tag{20}$$

with the boundary conditions $w(u^* \pm r_0) = \tilde{u}(u^* \pm r_0) = 0$. Let

$$\begin{aligned} f(r) &= \tilde{\lambda}\tilde{u}(r) r > 0 \\ g(r) &= \int_{u^*-r_0}^{r} f(r')dr > 0\,, \end{aligned} \tag{21}$$

we get

$$w(r) = \frac{\log r - \log(u^* - r_0)}{\log(u^* + r_0) - \log(u^* - r_0)} \int_{u^*-r_0}^{u^*+r_0} \frac{g(r')}{r'} dr + \int_{u^*-r_0}^{r} \frac{g(r')}{r'} dr' > 0\,. \tag{22}$$

This implies that $\bar{u} > \tilde{u}$ for $\forall r \in (u^* - r_0, u^* + r_0)$. Therefore we have the reconstructed surface $\bar{u}^{-1}(u^*)$ lies inside $\tilde{u}^{-1}(u^*)$. $\square$

The shrink in the fine feature will depends on magnitude of r_0.

Theorem 3.3. *Consider the following two dimensional case with the initial intensity image given by*

$$u_0 = \sqrt{x^2 + y^2}\,. \tag{23}$$

If $r_0 < u^*$, the regularized level surface $u^{-1}(u^*)$ stays inside the r_0-neighborhood of the original level surface $u_0^{-1}(u^*)$, i.e.

$$u^{-1}(u^*) \in \tilde{\Omega}_{r_0}\,. \tag{24}$$

Proof. This property comes from the maximum principle of the elliptic equation. Since

$$\min_{\partial\tilde{\Omega}_{r_0}} u_0 < u^* < \max_{\partial\tilde{\Omega}_{r_0}} u_0\,, \tag{25}$$

the maximum principle implies

$$\min_{\partial\tilde{\Omega}_{r_0}} u_0 < u|_{\tilde{\Omega}_{r_0}} < \max_{\partial\tilde{\Omega}_{r_0}} u_0\,, \tag{26}$$

and this leads to the conclusion. □

Theorem 3.4. *Consider the following two dimensional case with the initial intensity image given by*

$$u_0 = \sqrt{x^2 + y^2}\,. \tag{27}$$

The regularized level surface $u^{-1}(u^*)$ is smooth.

4 Numerical Method

In this section, we present a symmetric discretization to (11). For simplicity, we consider the following two dimensional case. It is straight-forward to generalize the discretization to higher dimensions. Let $g(x, y) = |\nabla u|^{-1}$. We apply the following symmetric discretization

$$\begin{aligned}\nabla\cdot(g\nabla u) \;=\;& g_{i+1/2,j}u_{i+1,j} + g_{i-1/2,j}u_{i-1,j} + g_{i,j+1/2}u_{i,j+1} + g_{i,j-1/2}u_{i,j-1} \\ & -(g_{i+1/2,j} + g_{i-1/2,j} + g_{i,j+1/2} + g_{i,j-1/2})u_{i,j}\,,\end{aligned} \tag{28}$$

where $g_{i\pm1/2,j\pm1/2}$ are regularized gradients given by

$$\begin{aligned}
g_{i+1/2,j} = g(x_{i+1/2}, y_j) &= \frac{1}{\sqrt{[D_x^+ u_0(x_i,y_j)]^2 + [D_y^0 u_0(x_i,y_j)]^2 + \epsilon^2}} \\
g_{i-1/2,j} = g(x_{i-1/2}, y_j) &= \frac{1}{\sqrt{[D_x^- u_0(x_i,y_j)]^2 + [D_y^0 u_0(x_i,y_j)]^2 + \epsilon^2}} \\
g_{i,j+1/2} = g(x_i, y_{j+1/2}) &= \frac{1}{\sqrt{[D_x^0 u_0(x_i,y_j)]^2 + [D_y^+ u_0(x_i,y_j)]^2 + \epsilon^2}} \\
g_{i,j-1/2} = g(x_i, y_{j-1/2}) &= \frac{1}{\sqrt{[D_x^0 u_0(x_i,y_j)]^2 + [D_y^- u_0(x_i,y_j)]^2 + \epsilon^2}}\,,
\end{aligned} \tag{29}$$

with ϵ to prevent division by zero, D^+, D^- and D^0 are the forward, the backward and the central differences, respectively. This results in a symmetric positive definite system of linear equations, which can be solved efficiently using any well-developed numerical method for solving a system of linear equations.

5 Example

5.1 Synthetic Objects

The clean surface in this example is given by

$$\begin{aligned} u_1(\mathbf{x}) &= 0.2 - \min(|x-0.35|, |y-0.65|, |z-0.5|) \\ u_2(\mathbf{x}) &= 0.2 - \min(|x-0.65|, |y-0.35|, |z-0.5|) \\ u_3(\mathbf{x}) &= 0.01 - \min(|x-0.75|, |y-0.75|, |z-0.5|) \\ u_4(\mathbf{x}) &= 0.1 - \min(|x-0.25|, |y-0.25|, |z-0.5|)\,. \end{aligned} \tag{30}$$

We have tried the following four different input surfaces. For the clean version, we have the clean surface defined by a distance function

$$u_0^{(1)}(\mathbf{x}) = \max(u_1, u_2, u_3, u_4)\,, \tag{31}$$

and the Heaviside version

$$u_0^{(2)}(\mathbf{x}) = H\left[\max(u_1, u_2, u_3, u_4)\right]\,. \tag{32}$$

With noise, we have

$$u_0^{(3)}(\mathbf{x}) = \max(u_1, u_2, u_3, u_4) + N(0,\sigma)\,, \tag{33}$$

where $N(0,\sigma)$ is the usual Gaussian noise with zero mean and standard deviation $\sigma = 0.01$. The corresponding Heaviside version is

$$u_0^{(4)}(\mathbf{x}) = H\left[\max(u_1, u_2, u_3, u_4) + N(0,\sigma)\right]\,. \tag{34}$$

With u_0 obtained with a Heaviside function, we use $u^* = 0.5$. For the cases with u_0 comes directly from the distance function, we have $u^* = 0$. The size of this data set is $128 \times 128 \times 128$. The total computational time for those clean examples are approximately 12 seconds implemented in MATLAB. For those noisy data, the Heaviside version takes around 63 seconds while the distance function case uses approximately 31 seconds.

5.2 Real Data

The resolution of each slice is 303×303 with totally 305 slices. It takes approximately 390 seconds to compute the solution in MATLAB.

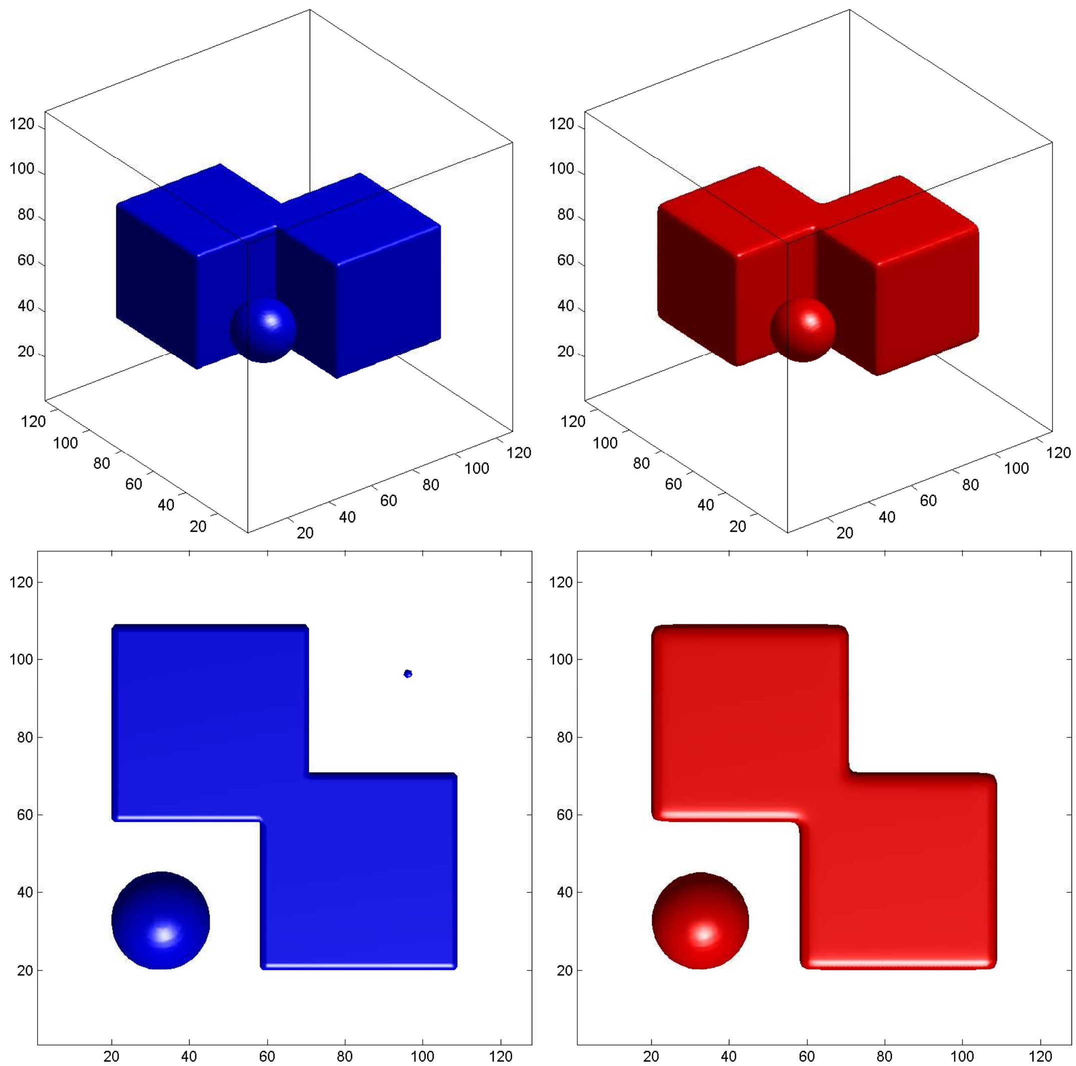

Figure 3: ($u_0^{(1)}$: clean distance function data) (Left) Original and (right) regularized.

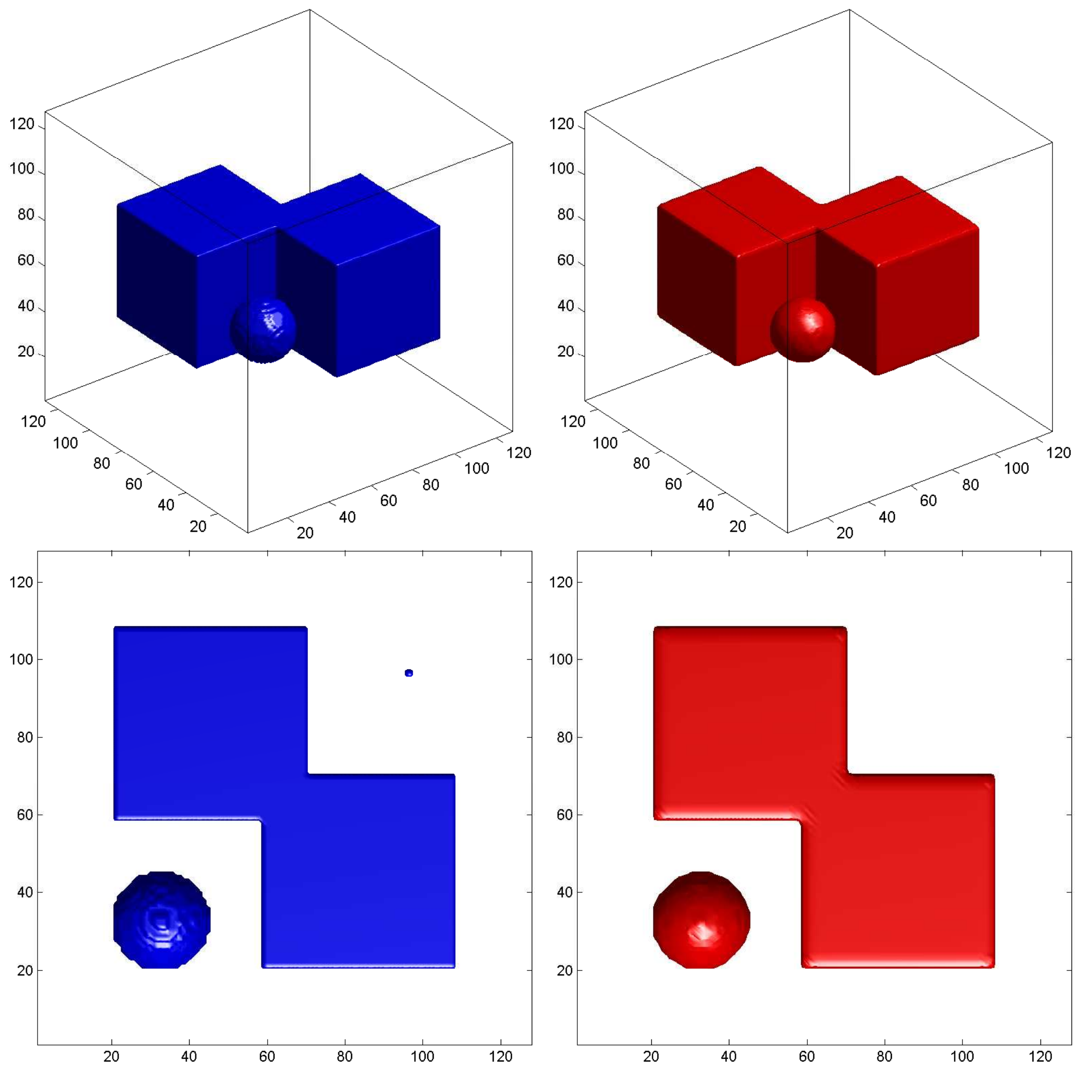

Figure 4: ($u_0^{(2)}$: clean heaviside data) (Left) Original and (right) regularized.

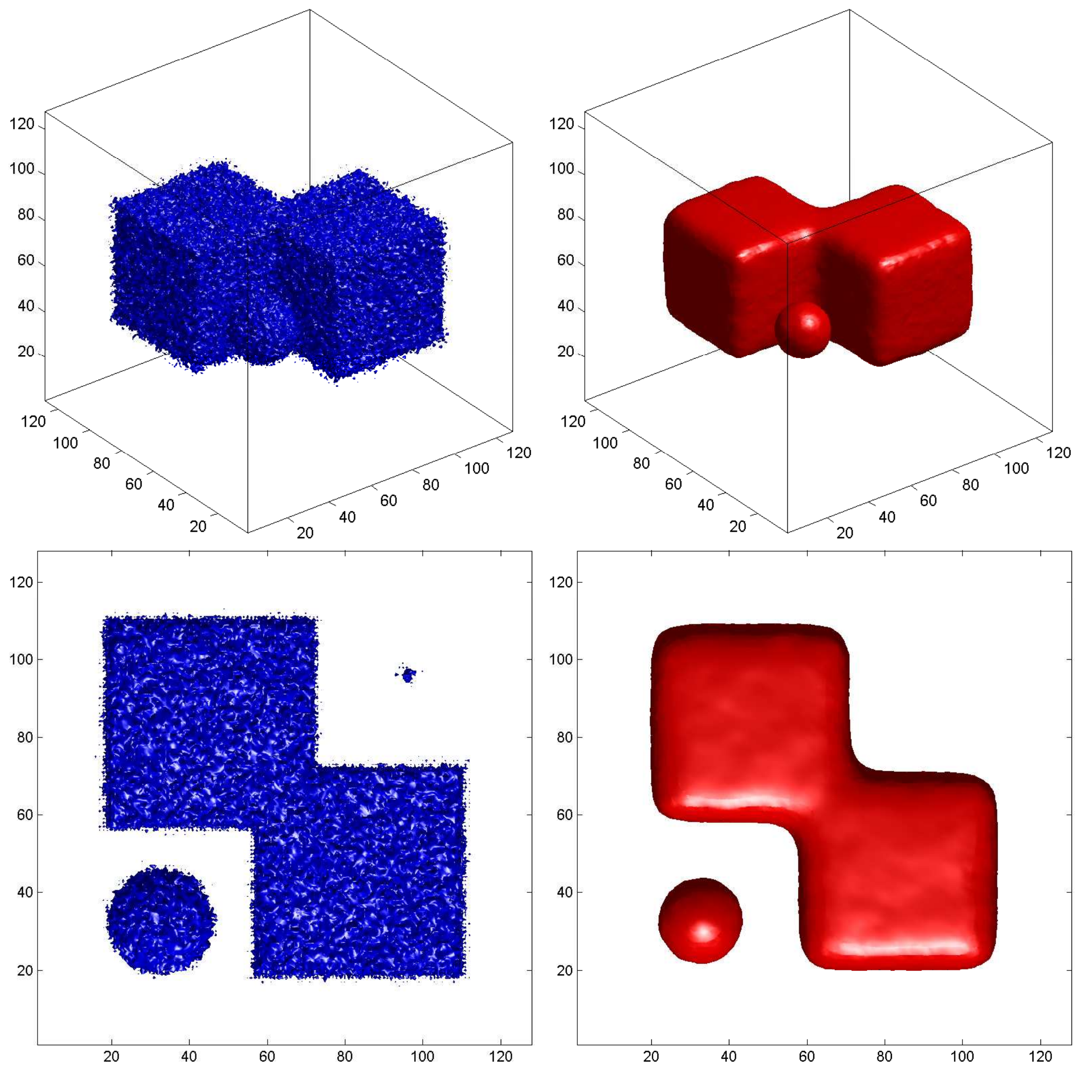

Figure 5: ($u_0^{(3)}$: noisy distance function data) (Left) Original and (right) regularized.

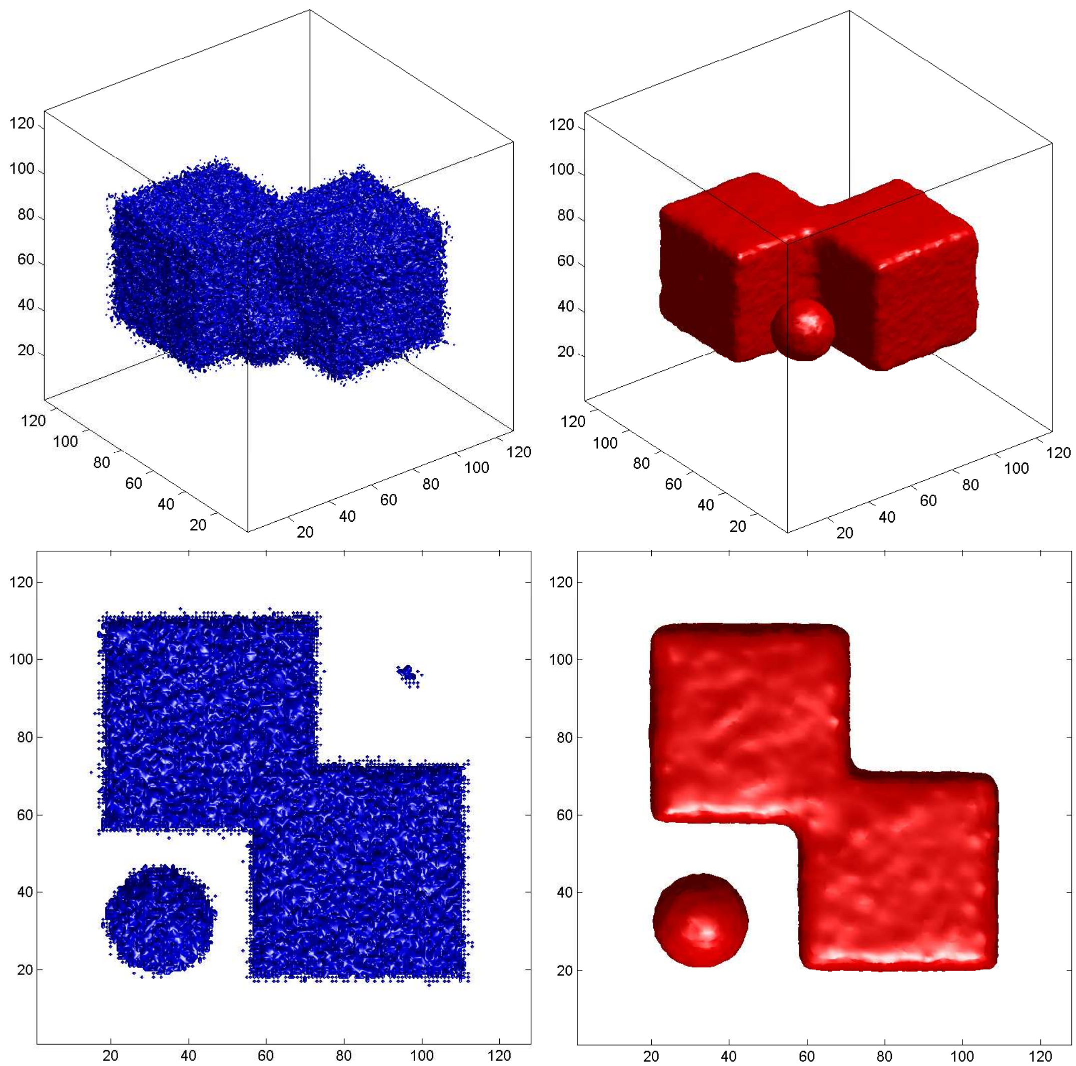

Figure 6: ($u_0^{(4)}$: noisy heaviside data) (Left) Original and (right) regularized.

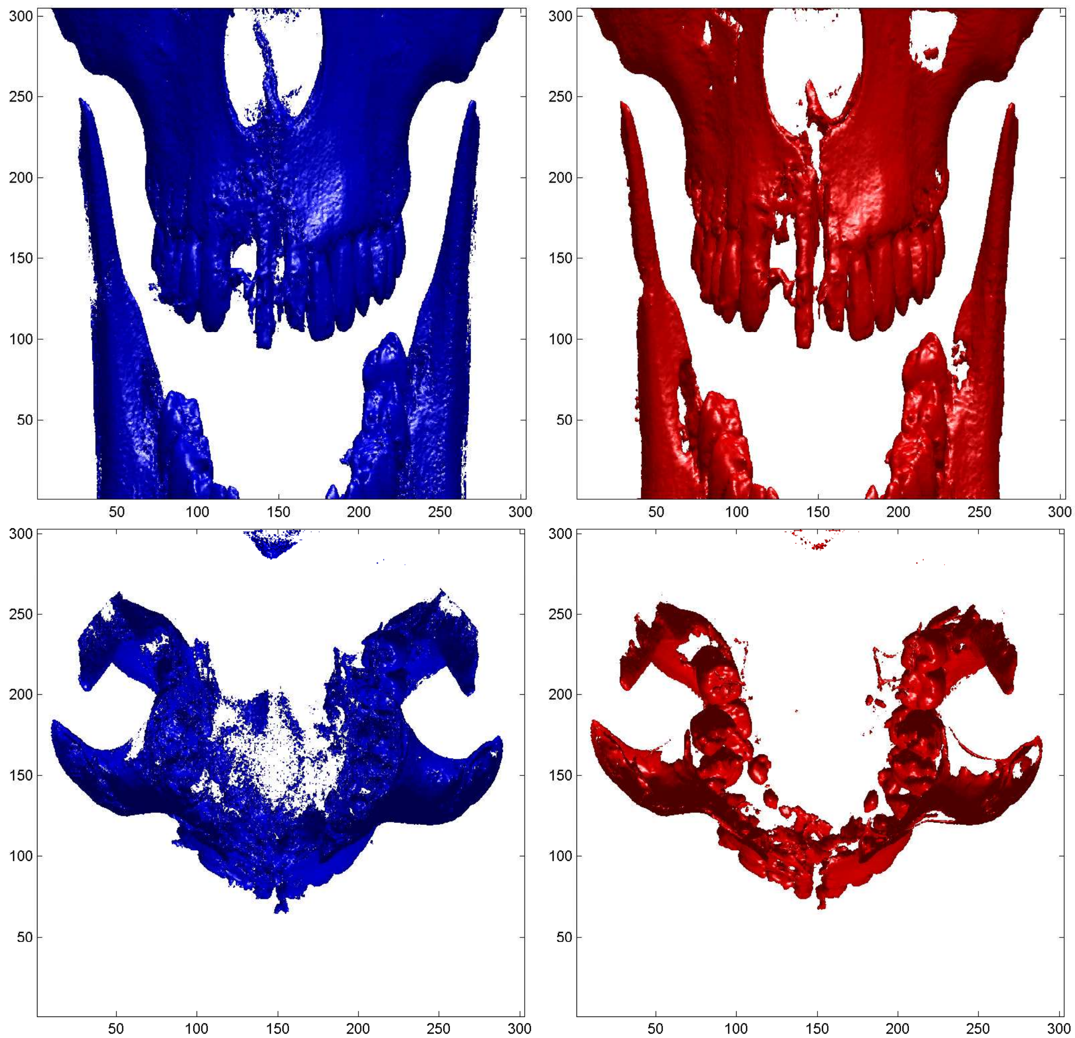

Figure 7: (Left) Original and (right) clean.

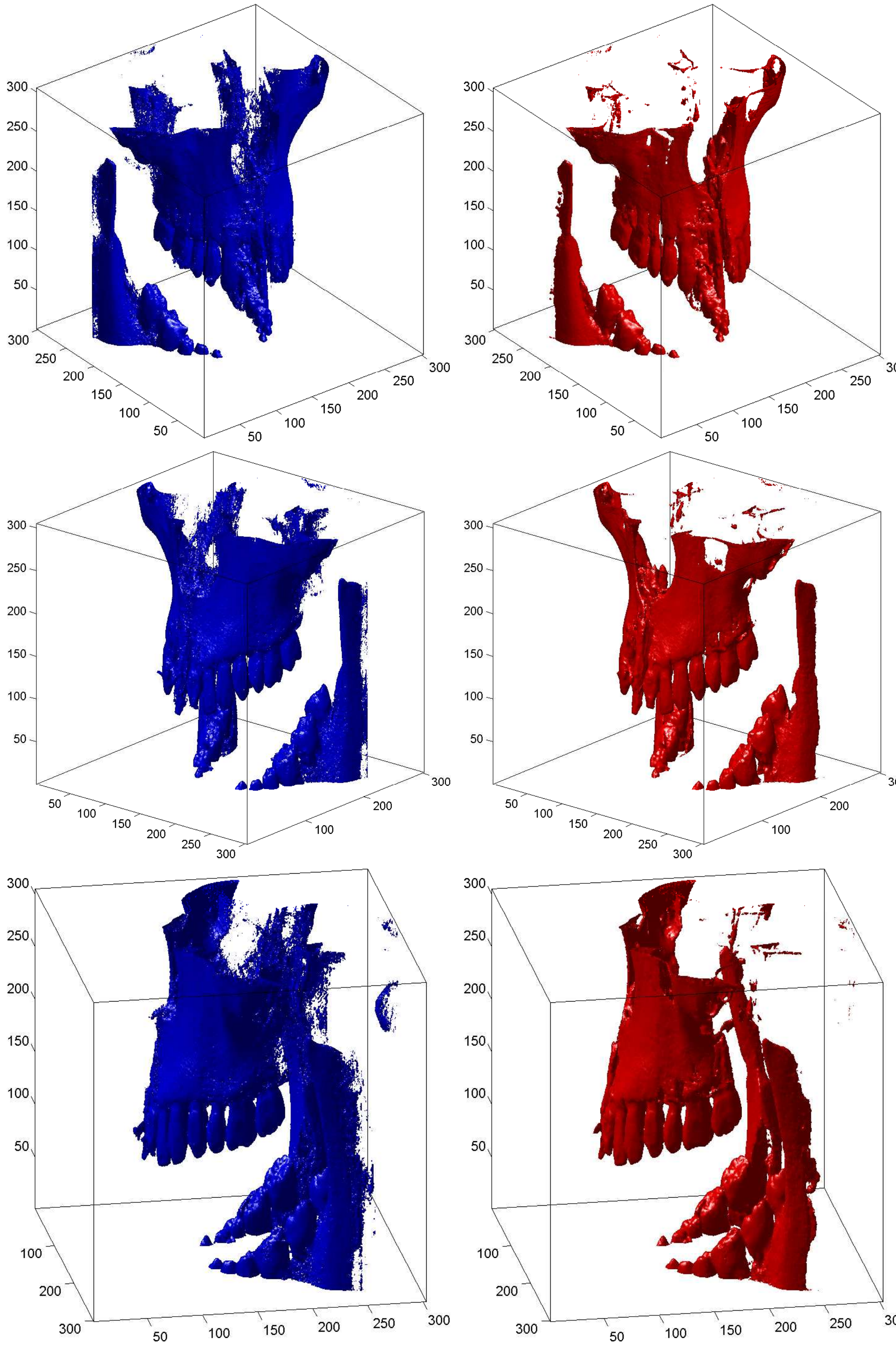

Figure 8: (Left) Original and (right) clean.

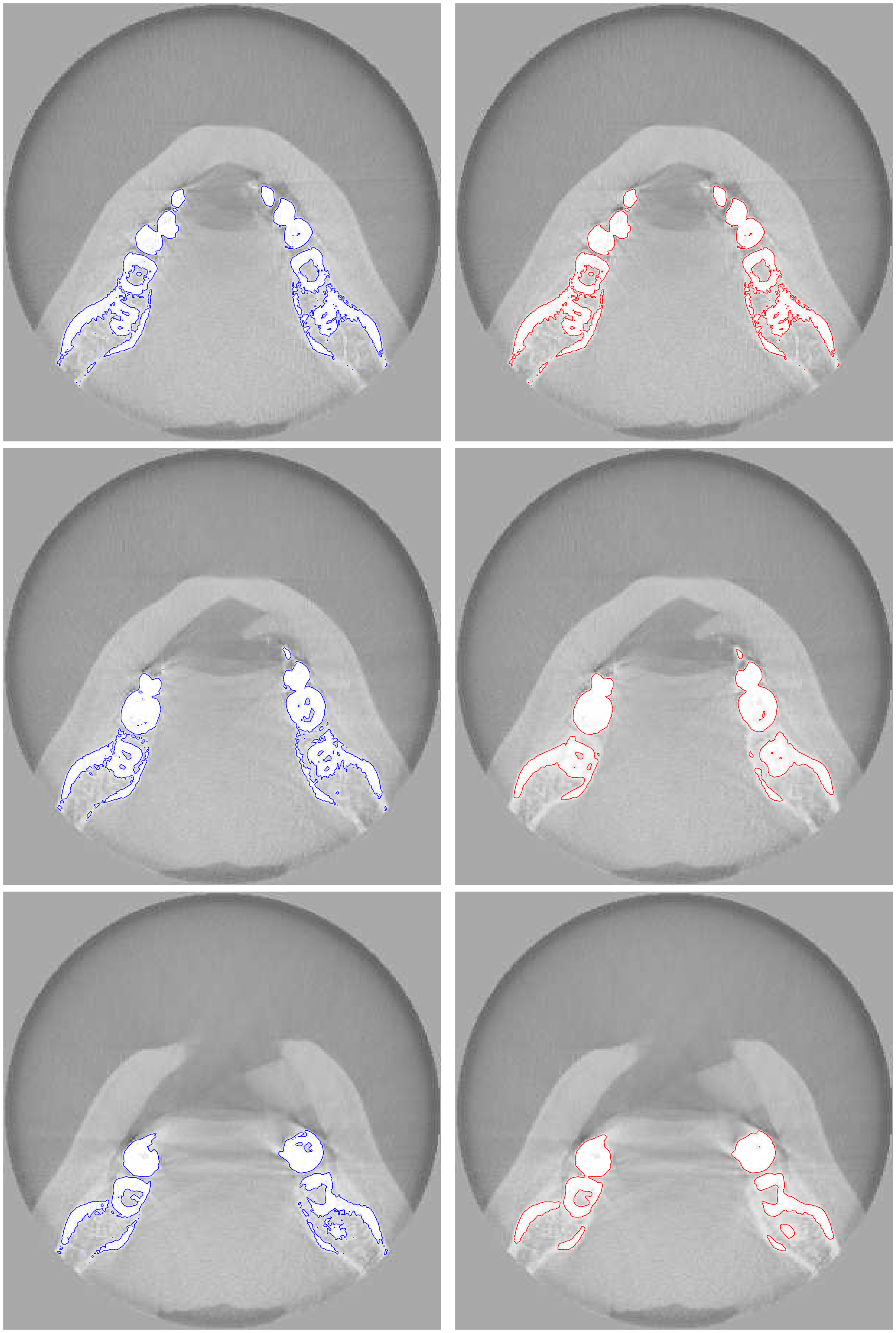

Figure 9: (Left) Original and (right) Clean. The intensity image should be very similar.

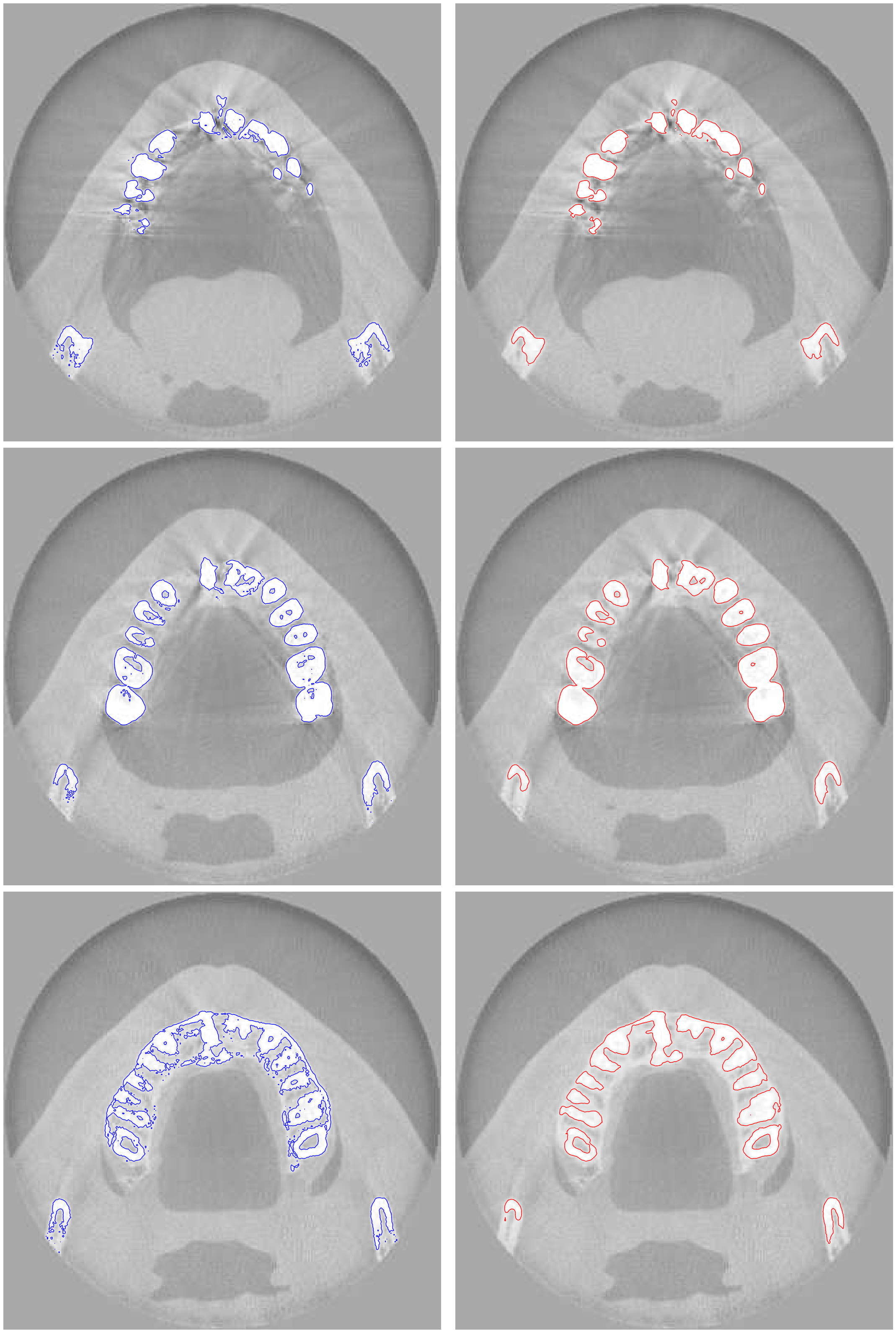

Figure 10: (Left) Original and (right) Clean. The intensity image should be very similar.

References

[1] A. Buades, A. Chien, J.M. Morel, and S. Osher. Topology preserving linear filtering applied to medical imaging. *CAM07-29, UCLA*, 2008.

[2] Y. Meyer. *Oscillating Patterns in Image Processing and Nonlinear Evolution Equations*. AMS, RI, 2001.

[3] L. Rudin, S.J. Osher, and E. Fatemi. Nonlinear total variation based noise removal algorithms. *Physica D*, 60:259–268, 1992.

[4] D. Strong and T. Chan. Edge-preserving and scale-dependent properties of total variation regularization. *Inverse Problems*, 19:S165–S187, 2003.